Pol. J. Environ. Stud. Vol. 33, No. 5 (2024), 5199-5209
DOI: *10.15244/pjoes/176798* ONLINE PUBLICATION DATE: 2024-06-10

Original Research

Surface Ozone in the Huaihe River Economic Belt, China: Spatial-Temporal Variations and Meteorological Driving Force

Xiaoyong Liu[1, 2], Yidan Zhang[1, 3], Feng Xu[1, 3], Feiyan Chen[1, 2], Hao Lin[1, 3], Jiqiang Niu[1, 2, 3]*

[1]School of Geographic Sciences, Xinyang Normal University, Xinyang 464000, China
[2]Henan Key Laboratory for Synergistic Prevention of Water and Soil Environmental Pollution, Xinyang Normal University, Xinyang 464000, China
[3]Henan Key Technology Engineering Research Center of Microwave Remote Sensing and Resource Environment Monitoring, Xinyang Normal University, Xinyang 464000, China

Received: 26 October 2023
Accepted: 11 December 2023

Abstract

Due to intense population density and rapid economic development, ozone (O_3) pollution is serious in the Huaihe River Economic Belt (HREB) of China. Based on pollutant and meteorological observation data from 2015 to 2020, many interdisciplinary methods, e.g., Kernel Density Estimation (KDE), Standard Deviation Ellipse (SDE), and Multiple Linear Regression (MLR), were employed to investigate the spatio-temporal distribution and the meteorological driving force of O_3 in 27 cities in the HREB. The results revealed that the annual mass concentration of O_3 increased in 2015~2018 and then decreased in 2019. The seasonal O_3 concentration displayed a bimodal structure, with highs in spring (122.3 μg/m^3) and summer (134.7 μg/m^3), and low in autumn (99.1 μg/m^3) and winter (64.4 μg/m^3). Spatially, the O_3 concentration in the northeastern HREB was higher than in the southwestern HREB. SDE analysis indicated that southeast Shangqiu (33.80°N-33.89°N, 116.33°E-116.40°E) was the center of gravity for O_3 concentrations in the HREB. The cities with severe O_3 pollution were clustered in the northern HREB, forming the high-high (HH) type, and those in the southern HREB with low O_3 concentrations forming the low-low (LL) type. Meteorological factors, including temperature, pressure, and sunshine duration, had a relatively significant impact on O_3 concentration. Based on the results of the MLR analysis, meteorological factors can explain 82.2%~18.2% (60.5% on average) of the O_3 variation in the HREB. The O_3 in the northern HREB was more affected by meteorological conditions than in the southern HREB.

Keywords: ozone, Huaihe River Economic Belt, spatial-temporal variations, meteorological factors

*e-mail: niujiqiang@xynu.edu.cn

Introduction

With accelerated urbanization and rapid economic development, fossil fuel consumption such as coal and oil increased substantially, causing serious fine particulate matter ($PM_{2.5}$) and ozone (O_3) pollution in China [1-3]. Atmospheric O_3 is mainly distributed in the upper stratosphere and troposphere. Stratospheric O_3 protects human health and the Earth's ecosystem by resisting ultraviolet light and insulation [4-6]. Surface O_3 is partially derived from stratospheric O_3 seepage and mostly from anthropogenic pollution such as emissions from motor vehicles and petrochemical industries [7-9]. O_3 is a secondary air pollutant, mainly produced by nitrogen oxides (NO_x) and volatile organic compounds (VOCs) through a series of photochemical reactions [10, 11]. Due to the irritating and strong oxidizing properties of O_3, high O_3 concentrations damage human health and the ecosystem [12]. Serious O_3 pollution has drawn much attention from the scientific community and the government [13-15]. Some studies revealed that hundreds of thousands of people die each year from respiratory diseases caused by O_3 pollution in China [16, 17]. Additionally, O_3 pollution is involved in crop photosynthesis and inhibits crop growth [18-20].

Numerous studies have shown that the type of air pollution in China is shifting from $PM_{2.5}$ to O_3. The synergistic effects of O_3 and $PM_{2.5}$ make air pollution more difficult to control [21-23]. Recent studies about O_3 pollution have focused on spatial and temporal variations, influencing factors, and effective control measures [24-26]. In the past few years, the O_3 concentration has been on a slow upward trend in China [27]. In some cities, O_3 has become the primary pollutant during the warm seasons [28, 29]. In recent years, O_3 pollution-related studies in China have mainly focused on economically developed regions such as Beijing-Tianjin-Hebei (BTH-UA), the Yangtze River Delta (YRD-UA), the Triangle of Central China (TC-UA), Chengdu-Chongqing (CY-UA), and the Pearl River Delta urban agglomeration [30]. Few studies have been aimed at the O_3 pollution in the HREB. The HREB is in eastern China, with a population accounting for 10% of the national total population. In addition to being an important grain-producing area in China, the HREB also has many industrial cities, including Rizhao, Zhengzhou, Fuyang, Bengbu, Linyi, Yancheng, and Xvzhou [31, 32]. Liu et al. found that both meteorological conditions and precursor emissions affect ozone concentration changes in the Huaihe River Basin [33].

This study aimed to investigate the spatial-temporal distribution and meteorological driving forces on O3 variation in the HREB by using a multi-method approach, specifically: (1) the annual, seasonal, monthly, and diurnal variations of O3 concentrations were systematically described' (2) the spatial variation of O3 was analyzed; and (3) the meteorological driving forces were estimated. The study results contributed to a further understanding of the spatial-temporal patterns and mechanisms of O_3 pollution in the HREB. Further, the findings provided a scientific basis for the O_3 control measures in the HREB.

Materials and Methods

Study Area

The HREB (30.9°N-36.2°N, 112.2°E-121.0°E) is located in central China (Fig. 1), including 27 cities: Luohe, Pingdingshan, Xuchang, Xinyang, Zhoukou, Zhumadian, and Zhengzhou in Henan Province, Bengbu, Bozhou, Fuyang, Huaibei, Hefei, Huainan, Luan, and Suzhou in Anhui Province, Heze, Jining, Linyi, Rizhao, and Zhaozhuang in Shandong Province, Huaian, Lianyungang, Suqian, Xvzhou, and Yancheng in Jiangsu Province. Among them, Zhengzhou is the capital city of Henan Province, with a huge population [34]. As a resource-based industrial city in Henan Province, Pingdingshan has abundant coal resources. Hefei, the capital of Anhui Province, is one of the megacities in China. Xuzhou is an important coal and power production area in China. The HREB covers about 205, 000 km^2 with a population of about 180 million [35]. The line of the Qinling Mountain and Huaihe River is the boundary between the temperate and subtropical zones of China, as well as between the subtropical and temperate monsoon climates.

Materials

Hourly O_3 mass concentration data from 2015 to 2020 was obtained from the China National Environmental Monitoring Centre, published by the Ministry of Ecology and Environment of the People's Republic of China. The daily maximum 8-h sliding average of O_3 concentration ($MDA8\text{-}O_3$) was used to represent the daily average O_3 concentration. Meteorological data, including temperature, pressure, precipitation, wind speed, wind direction, and sunshine duration, were derived from the China Science and Technology Resources Sharing Network published by the National Science and Technology Infrastructure Platform Centre.

Methods

Kernel Density Estimation

The annual O_3 concentration was analyzed using Kernel Density Estimation. The Kernel Density Estimation uses "shocks" instead of "boxes" in the histogram, so it is smoothed. Smoothing is achieved by giving small weights to the observations far from the point being estimated. The Kernel Density Estimation for a sequence X at point x is given by:

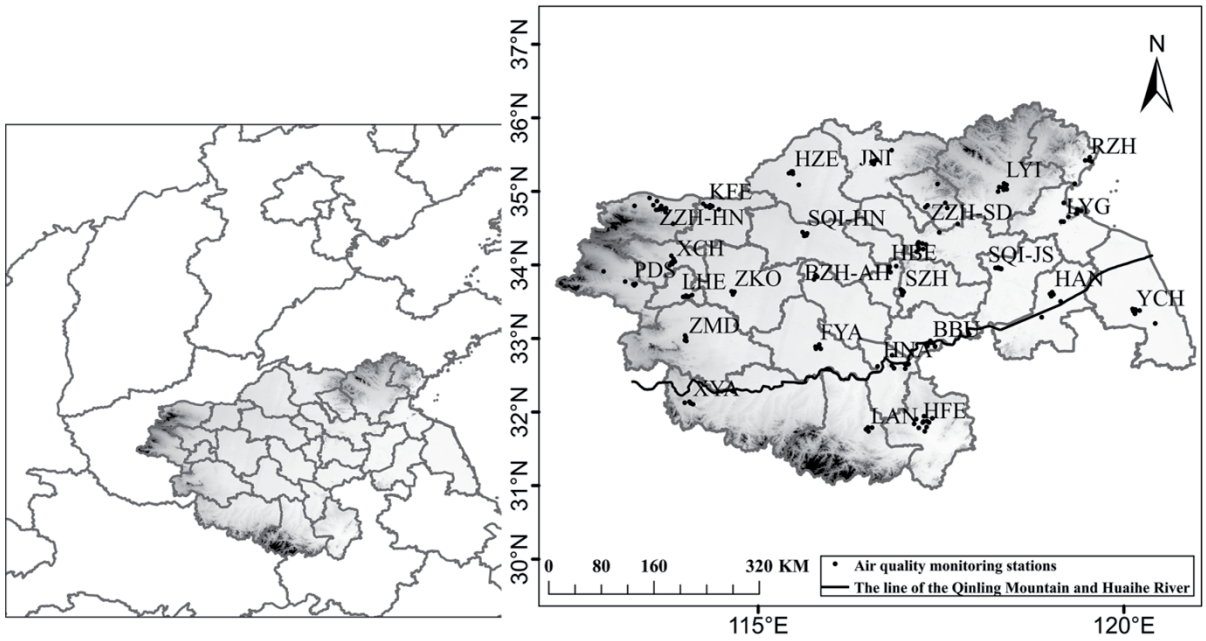

Fig. 1. Location and cities of the Huaihe River Economic Belt (HREB) in China (BBU: Bengbu, BZH: Bozhou, FYA: Fuyang, HAN: Huaian, HBE: Huaibei, HFE: Hefei, HNA: Huainan, HZE: Heze, JNI: Jining, KFE: Kaifeng, LAN: Luan, LHE: Luohe, LYG: Lianyungang, LYI: Linyi, PDS: Pingdingshan, RZH: Rizhao, SQI-HN: Shangqiu, SQI-JS: Suqian, SZH: Suzhou, XCH: Xuchang, XYA: Xinyang, XZH: Xvzhou, YCH: Yancheng, ZKO: Zhoukou, ZMD: Zhumadian, ZZH-HN: Zhengzhou, ZZH-SD: Zhaozhuang). The black dots represent O_3 monitoring sites.

$$f(x) = \frac{1}{Nh}\sum_{i=1}^{N} K\left(\frac{x - X_i}{h}\right) \tag{1}$$

Where N is the number of observations, h indicates the bandwidth (or smoothing parameter), and K represents the kernel function [36].

Standard Deviational Ellipse

A standard deviation ellipse (SDE) was used to investigate the interannual spatial changes of O_3 concentrations. The SDE is one of the geostatistical methods that can accurately reveal the spatial distribution characteristics of various geographic elements. SDE calculates the center of gravity by using a weighted average center, averaging the coordinates of each point, and providing weights based on ecological spatial density attribute variables. The calculation is defined as:

Weighted average center:

$$\bar{X}_\omega = \frac{\sum_{i=1}^{n} \omega_i x_i}{\sum_{i=1}^{n} \omega_i}, \bar{Y}_\omega = \frac{\sum_{i=1}^{n} \omega_i y_i}{\sum_{i=1}^{n} \omega_i} \tag{2}$$

Elliptical direction:

$$\tan\theta = \frac{A + B}{C} \tag{3}$$

$$A = \left(\sum_{i=1}^{n} \omega_i^2 \tilde{x}_i^2 - \sum_{i=1}^{n} \omega_i^2 \tilde{y}_i^2\right) \tag{4}$$

$$B = \sqrt{\left(\sum_{i=1}^{n} \omega_i^2 \tilde{x}_i^2 - \sum_{i=1}^{n} \tilde{y}_i^2\right)^2 + 4\sum_{i=1}^{n} \omega_i^2 \tilde{x}_i^2 \, \tilde{y}_i^2} \tag{5}$$

$$C = 2\sum_{i=1}^{n} \omega_i^2 \tilde{x}_i \, \tilde{y}_i \tag{6}$$

x-axis standard deviation:

$$\sigma_x = \sqrt{\frac{\sum_{i=1}^{n} (\omega_i \tilde{x}_i \cos\theta - \omega_i \tilde{y}_i \sin\theta)^2}{\sum_{i=1}^{n} \omega_i^2}} \tag{7}$$

y-axis standard deviation:

$$\sigma_y = \sqrt{\frac{\sum_{i=1}^{n} (\omega_i \tilde{x}_i \sin\theta - \omega_i \tilde{y}_i \cos\theta)^2}{\sum_{i=1}^{n} \omega_i^2}} \tag{8}$$

Where (x_i, y_i) are the spatial coordinates of the object of study. ω_i indicates the weight at spatial element i. $(\bar{X}_i, \bar{Y}_i)$ is the weighted average center of the spatial data set of the study object. θ is the azimuth of the ellipse, and $\tilde{x}_i$ and $\tilde{y}_i$ are the coordinate deviations from the spatial coordinates of the study object to the mean

center. σ_x and σ_y is the standard deviation of the x-axis and y-axis [37].

Global and Local Spatial Autocorrelation Analysis

Spatial autocorrelation, a statistical method to study the correlation between the whole space and each unit within it, is mainly used to describe the spatial aggregation characteristics of the study area. Spatial autocorrelation can be divided into two statistical types, i.e., global spatial autocorrelation and local spatial autocorrelation. In this study, global spatial autocorrelation was used to analyze the spatial distribution of O_3 concentrations across the HREB. Specifically described in terms of the global Moran's I, which is calculated as:

$$I = \frac{n}{\sum_{i=1}^{n}(X_i - \bar{X})^2} \cdot \frac{\sum_{i=1}^{n}\sum_{j=1}^{n} W_{ij}(X_i - \bar{X})(X_j - \bar{X})}{\sum_{i=1}^{n}\sum_{j=1}^{n} W_{ij}} \quad (9)$$

Where I is Moran's I statistic, n is the total number of study areas, X_i is the observed value of some attribute x on spatial cell i, W_{ij} is the normalized spatial weight matrix to represent the spatial location relationship between each spatial cell [38], and $\bar{X}$ is the average value of an attribute feature x over n study regions.

The Moran's I of global spatial autocorrelation takes a value between -1 and 1. If Moran's I is greater than 0, it indicates spatially positive, which indicates that the attribute values are spatially aggregated. If Moran's I is less than 0, then a negative spatial correlation is indicated, indicating significant differences in the spatial distribution. If Moran's I is equal to 0, it suggests spatial uncorrelated, i.e., attribute values are spatially randomly distributed.

Local spatial autocorrelation is a measure of the spatial association and degree of difference between each internal spatial unit and neighboring spatial units. Moran scatter plots are generally used to perform local autocorrelation analysis. Regions that pass the significance test at a given level of significance are presented by LISA aggregation plots [39].

Pearson Test

The correlation coefficient is a quantity used to determine the degree of linear correlation between multiple variables. The larger the Pearson's correlation coefficient, the closer the relationship. In the present study, the Pearson test is used to describe the relationship between the O_3 concentration and various meteorological factors.

Multivariable Linear Regression

Based on the multivariable linear regression (MLR) model, the meteorological data for each station, including Temperature (T), Pressure (P), Relative Humidity (RH), Precipitation (Pre), Wind Speed (WS), Wind Direction (WD), and Sunshine Duration (SSD) used as independent variables to discuss the explanation of meteorological factors for O_3 changes. The calculation is defined as:

$$Y = F(\alpha, \beta, \gamma, \lambda, \phi, \nu, \mu) + \sigma \quad (10)$$

Where $F(\alpha, \beta, \gamma, \lambda, \phi, \nu, \mu)$ suggests the O_3 density influenced by T, P, RH, Pre, WS, WD, and SSD; σ is the residual term, indicating the effect of factors such as topography and random error.

Results and Discussion

Temporal Variations in O_3 in the Huaihe River Economic Belt

Annual Variation

China's Ambient Air Quality Standards (AAQS) set the following limits for the 8-hour average concentration of ozone, i.e., the primary standard (100 ug/m³) and the secondary standard (160 ug/m³). Fig. 2 shows the kernel density estimates and exceedance rates of O_3 concentrations in the HREB from 2015 to 2020. Overall, the annual average O_3 concentration in the HREB (90th percentile of MDA8-O_3) gradually increased from 2015, then showed a slight downward trend in 2019 and 2020. O_3 pollution remained a serious problem in the HREB. Specifically, the annual average O_3 concentration in 2018 was 179.0 μg/m³, an increase of 14.0% compared to 2015 (157.0 μg/m³). Compared to 2018, O_3 concentrations in 2019 (178.0 μg/m³) and 2020 (163.0 μg/m³) decreased by 0.6% and 8.4%, respectively. The State Council of the People's Republic of China published the "Three-Year Action Plan for Winning the Blue Sky Defense War" (Plan) in June 2018. The Plan proposes that governments set stringent emission standards for industrial enterprises, in addition to strengthening the control of motor vehicle exhaust. According to previous studies [30], O_3 concentrations in some major cities in China showed a downward trend from the 2019 year [27]. A decreasing trend in O_3 concentrations in the HREB from 2019 was also found in this study, indicating that O_3 pollution control measures worked.

As displayed in Fig. 2a), the kernel density curves of O_3 concentrations were single-peaked in all years except for 2019, which is double-peaked. The change in the kernel density curve over time showed a shift to the right in the center as well as in the interval of change, with a small expansion in width. The height of the main peak of the kernel density curve showed a decreasing trend before 2019, followed by an increasing trend, which suggested O_3 pollution has been reduced. The persistent increase in O_3 pollution concentrations from 2015 to 2018 was largely caused by anthropogenic factors such as the

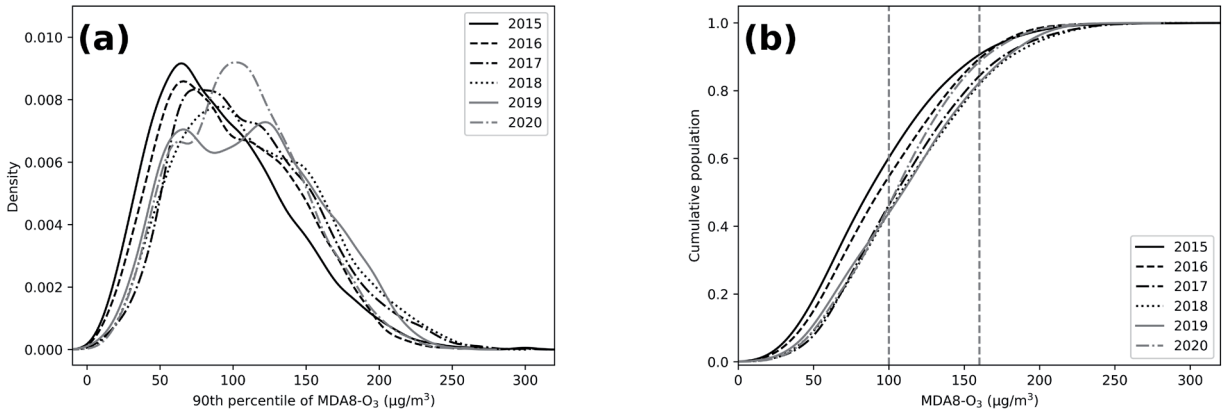

Fig. 2. a) Kernel-density estimates of annual mean O_3 concentrations and b) the annual over-standard rate of the O_3 concentrations in the HREB in 2015-2020.

increasing motor vehicle and petrochemical industries in China [30]. The kernel density curve in 2019 exhibited a double peak, and both peaks were reduced. Overall, O_3 concentration decreased in 2019. This suggests that the Plan has been effective in the HREB. O_3 concentrations displayed a significant increase in 2020. The lockdown during the COVID-19 epidemic in 2020 reduced anthropogenic emissions, resulting in a decrease in $PM_{2.5}$ concentration. The decrease in $PM_{2.5}$ concentration enhances solar radiation, leading to an increase in O_3 concentration [14]. The proportions of MAD8-O_3 exceeded the Chinese National Ambient Air Quality Standard I (CAAQS Class I; 100 μg/m^3) in the HREB were 39.4%, 45.0%, 53.2%, 55.3%, 55.7%, and 58.9% from 2015 to 2020, respectively (Fig. 2b). This indicated that the increase in O_3 concentration in the HREB slowed down, but O_3 pollution is still relatively serious.

Monthly Variation

The monthly O_3 concentration displayed an M-shaped bimodal variation with peaks in June, (155.3 μg/m^3) and September (131.0 μg/m^3) (Fig. 3a). It was found that the monthly O_3 variation was related to the latitude in China, with a single-peaked structure usually found at latitudes above 35°N, while in most cases, a double-peaked structure is found south of 35°N [22, 40]. The latitude of the HREB is 31.7°N-35.4°N, and the bimodal structure of the O_3 monthly variation in the study was the same as the results of previous studies. As shown in Fig. 3b, the seasonal averages of O_3 concentrations in the HREB in spring, summer, autumn, and winter from 2015 to 2020 were 122.3, 134.7, 99.1, and 64.4 μg/m^3, respectively. The O_3 concentrations in the HREB demonstrated a characteristic of "high in spring and summer, low in autumn and winter", which was consistent with the overall seasonal trend of O_3 in East Asia. In summer, relatively high temperatures and intense radiation enhance photochemical reactions, which lead to increased O_3 production [34].

Diurnal Variation

The diurnal variation of O_3 concentration displayed a single-peak characteristic in the HREB (Fig. 4),

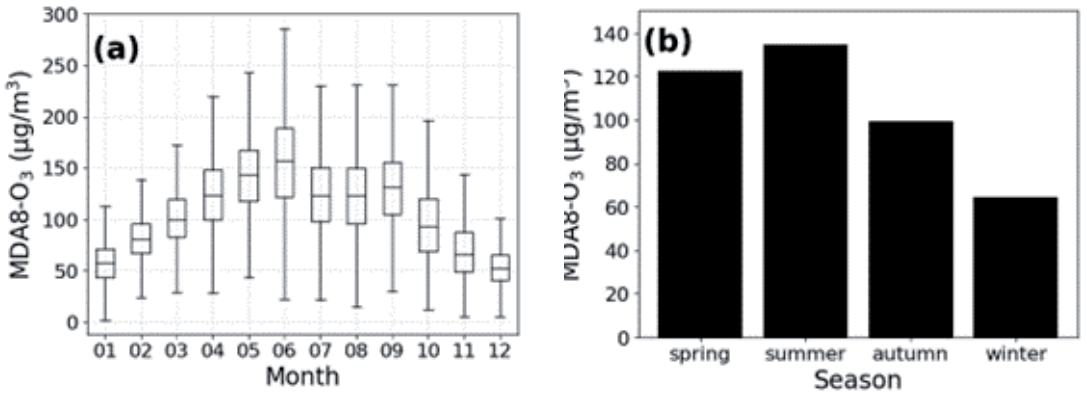

Fig. 3. a) Monthly and b) seasonal variation of MDA8-O_3 in the HREB over 2015-2020. Shown are the average value (central horizontal bar within the boxes), 25th and 75th percentiles (lower and upper bars of the boxes, respectively), and minimum and maximum (lower and upper whiskers, respectively).

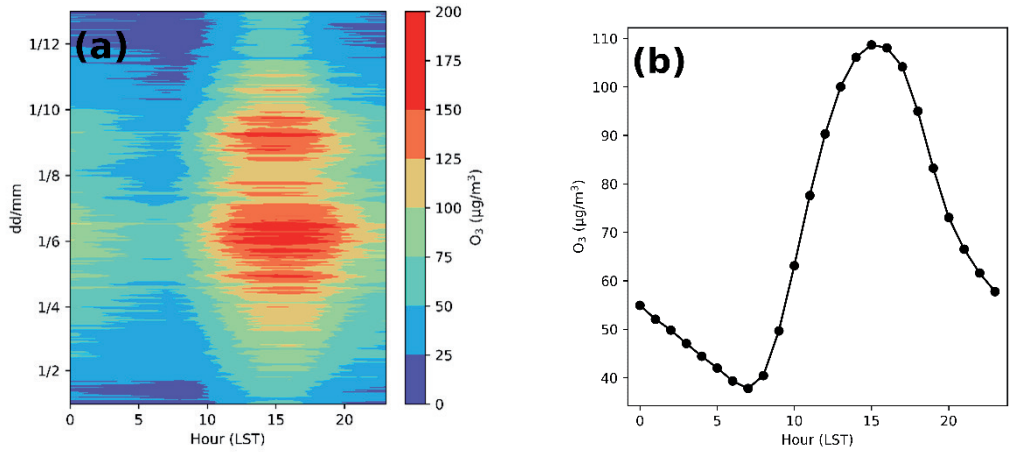

Fig. 4. Diurnal variations of O_3 concentrations in the HREB during 2015-2020.

with high levels during the day and low levels at night. As shown in Fig. 4a), O_3 concentrations remained high at 20:00 (LT) during May-July. In June, O_3 concentrations above 150 μg/m^3 lasted for about 10 hours per day. During the daytime, with the rising sun and enhanced solar radiation, precursors such as VOCs and NO_x participate in photochemical reactions and contribute to the formation of O_3. As shown in Fig. 4b), the daily O_3 maximum occurred at 15:00 (108.7 μg/m^3) and the minimum at 7:00 (37.8 μg/m^3). O_3 concentration increased from 7:00 and decreased from 15:00. At night, the NO_x titration reaction decreased the O_3 concentration [41]. The time when the daily minimum and maximum O_3 concentrations occurred was 1 hour after the average sunrise time and the average daily maximum temperature time, respectively.

Spatial Variations in O_3 in the HREB

Standard Deviational Ellipse

The general changes in O_3 spatial pattern in the HREB in different years were characterized by SDE analysis. As shown in Fig. 5, the annual O_3 concentrations were mainly distributed in the southwest-northeast direction of the HREB. The azimuth of the ellipse increased from 84.10° in 2015 to 85.12° in 2018 and then decreased to 84.66° in 2020 (Table 1). Most developed cities in China are in the eastern coastal areas, and high O_3 levels are usually found in those cities. The direction of movement of the ellipse was first to the southeast and then to the northwest (Fig. 5), which suggested the difference in O_3 concentration

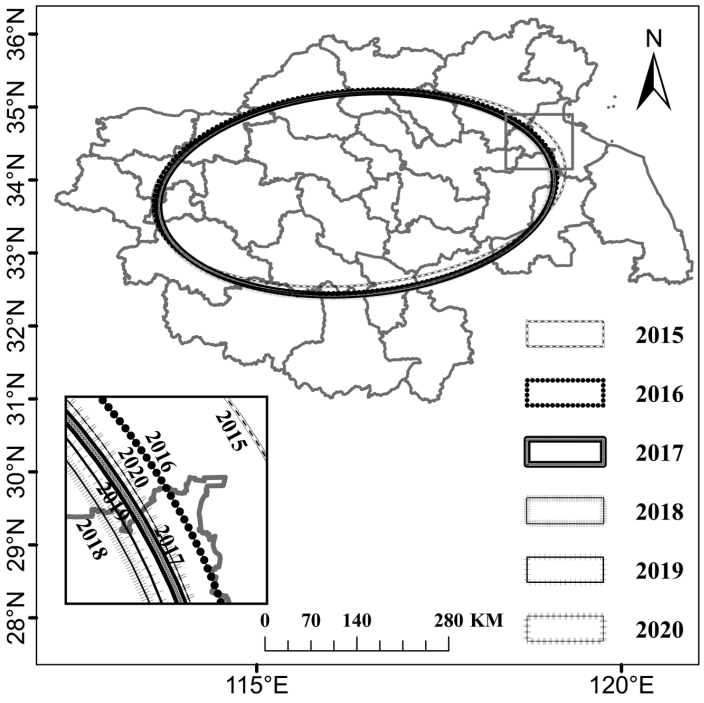

Fig. 5. Standard ellipse deviation distribution in different years.

Table 1. Parameters of the standard deviation ellipse in the Huaihe River Economic Belt (HREB).

Items	Variables	Parameters				
		Center X	Center Y	Minor axes/km	Major axes/km	Rotation
Year	2015	116.40°E	33.89°N	132.87	284.77	84.10°
	2016	116.35°E	33.84°N	138.22	277.34	85.07°
	2017	116.37°E	33.81°N	137.87	271.62	85.11°
	2018	116.33°E	33.80°N	138.97	271.23	85.12°
	2019	116.33°E	33.82°N	137.06	272.85	84.84°
	2020	116.36°E	33.82°N	138.30	272.93	84.66°

between inland and coastal cities was decreasing. The mean center detected by SDE in the HREB was in southeastern Shangqiu. From 2015 to 2018, the center moved from 33.89°N, 116.40°E, to 33.80°N, 116.33°E, which indicated a greater decrease in O_3 concentration in the northwestern part of the HREB. From 2018 to 2020, the center of O_3 concentration in the HREB shifted from 33.80°N, 116.33°E, to 33.82°N, 116.36°E, which suggested a greater decrease in O_3 concentration in the southwestern part of the HREB. The decrease in O_3 concentration in the HREB mainly occurred in its western inland cities, which was similar to the O_3 variations on a national scale [7]. The long axis of the ellipse decreased from 284.77 km in 2015 to 271.23 km in 2018, following a small increase in 2019 and 2020. The change in the long axis illustrated the spatial aggregation trend and spatial variation of O_3 concentrations from 2015 to 2020. The ratio between the long and short axes of the ellipse showed a decreasing trend from 2015 to 2018, indicating a weakening trend of the directional distribution. Then the ratio increased in 2019 and decreased in 2020. In 2020, due to the influence of COVID-19, anthropogenic activities reduced remarkably, causing a decrease in the variability of O_3 pollution among cities.

Spatial Autocorrelation of O_3 Concentrations

Global Moran's I was calculated for different years and seasons in the HREB to discuss the spatial correlation of O_3. From 2015 to 2020, the annual Moran's I was 0.35, 0.40, 0.13, 0.18, 0.18, and 0.07, respectively. The seasonal Moran's I was 0.21, 0.45, 0.45, and 0.41, respectively. The positive Moran's I indicates positive spatial autocorrelation and spatial aggregation of O_3 concentrations in the HREB, which suggests that O_3 in cities may be influenced by their neighboring cities. The highest global Moran's I in the HREB was found in autumn (0.452), followed by summer (0.449), indicating an enhanced aggregation of O_3 concentrations. Therefore, it is necessary to carry out cross-city cooperation to control O_3 pollution.

To identify the distribution and aggregation patterns of O_3 pollution in cities in the HREB, a local spatial autocorrelation analysis was employed in this study. As shown in Fig. 6b), the most polluted cities were distributed in the northern part of the HREB, forming a high-high (HH) type of O_3 concentration. Cities with HH concentrations included Heze, Jining, and Zaozhuang. These cities are located north of the HREB, having less precipitation and high energy consumption. Most of the surrounding cities are industrial cities with

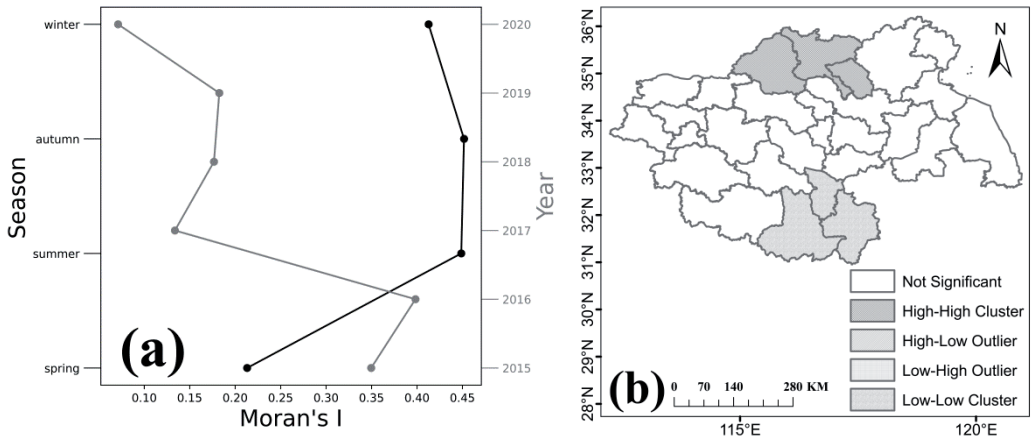

Fig. 6. a) Global Moran's I index and b) spatial agglomeration of O_3 concentrations in the HREB in 2015-2020.

intensive anthropogenic emissions. The southern cities in the HREB have low O_3 concentrations and have formed a low-low (LL) type. Cities with LL concentrations include Huainan, Luan, and Hefei. These cities are in the southern part of the HREB with abundant precipitation, which reduces O_3 production. In conclusion, the agglomerated O_3 pollution needs to be managed by joint efforts among cities, and more stringent measures should be taken in the northern part of the HREB.

Meteorological Driving Force

The correlation between individual meteorological factors and O_3 concentration is listed in Table 2. O_3 concentration showed a positive correlation with *T* and SSD in each city. This result is the same as that of the previous study [33]. The surface O_3 is mainly generated by precursors through photochemical reactions, so O_3 is sensitive to temperature and solar radiation [30]. Except for a positive correlation with RH in Rizhao, O_3 concentration showed negative correlations with *P*, RH, and Pre in each city, among which the correlation with Pre in Rizhao and Zhengzhou was not significant. Rizhao is located east of the Yellow Sea and has a temperate monsoon climate with high precipitation and a humid climate. It is presumed that the correlation is not significant due to the prevalence of Pre and RH. Zhengzhou has a temperate continental climate with

Table 2. Correlation coefficients between O_3 and meteorology for 27 cities in the HREB.

City	Pearson Correlation						
	T	*P*	RH	Pre	WS	WD	SSD
LYI	0.75**	-0.64**	-0.05*	-0.06**	-0.09**	0.16**	0.45**
BZH-AH	0.61**	-0.51**	-0.22**	-0.09**	-0.03	-0.00	0.49**
XYA	0.61**	-0.47**	-0.42**	-0.17**	0.00	0.07**	0.55**
LAN	0.57**	-0.45**	-0.29**	-0.09**	-0.10**	-0.08**	0.46**
HFE	0.63**	-0.54**	-0.29**	-0.15**	-0.05*	-0.03	0.55**
ZKO	0.74**	-0.63**	-0.25**	-0.06**	0.02	-0.03	0.53**
SQI-HN	0.72**	-0.64**	-0.16**	-0.05*	-0.06**	0.13**	0.51**
SZH	0.40**	-0.35**	-0.12**	-0.04	0.05*	0.04	0.33**
SQI-JS	0.70**	-0.60**	-0.18**	-0.07**	-0.06**	0.10**	0.46**
PDS	0.77**	-0.67**	-0.14**	-0.06**	-0.09**	-0.04*	0.55**
KFE	0.73**	-0.66**	-0.19**	-0.07**	0.05*	0.18**	0.50**
XZH	0.70**	-0.61**	-0.29**	-0.09**	-0.01	0.01	0.52**
RZH	0.65**	-0.58**	0.12**	-0.03	-0.18**	0.15**	0.33**
ZZH-SD	0.74**	-0.64**	-0.20**	-0.08**	-0.07**	0.04	0.45**
JNI	0.79**	-0.70**	-0.19**	-0.05*	0.05*	-0.04	0.49**
HBE	0.70**	-0.60**	-0.23**	-0.07**	-0.03	-0.01	0.51**
HNA	0.60**	-0.58**	-0.23**	-0.10**	0.12**	0.00	0.52**
HAN	0.63**	-0.55**	-0.18**	-0.09**	-0.07**	0.11**	0.46**
LHE	0.74**	-0.65**	-0.29**	-0.08**	-0.12**	0.03	0.54**
YCH	0.52**	-0.46**	-0.26**	-0.09**	-0.08**	0.03	0.45**
HZE	0.74**	-0.66**	-0.23**	-0.06**	0.02	0.08**	0.56**
BBU	0.63**	-0.52**	-0.31**	-0.09**	-0.15**	0.07**	0.54**
XCH	0.75**	-0.69**	-0.16**	-0.05*	-0.09**	0.11**	0.50**
LYG	0.59**	-0.54**	-0.07**	-0.06*	0.02	-0.12**	0.43**
ZZH-HN	0.80**	-0.73**	-0.15**	-0.03	0.11**	0.01	0.48**
FYA	0.63**	-0.52**	-0.32**	-0.10**	-0.15**	-0.06**	0.52**
ZMD	0.70**	-0.61**	-0.26**	-0.11**	-0.12**	-0.09**	0.50**

** Correlation is significant at the 0.01 level (2-tailed), * Correlation is significant at the 0.05 level (2-tailed).

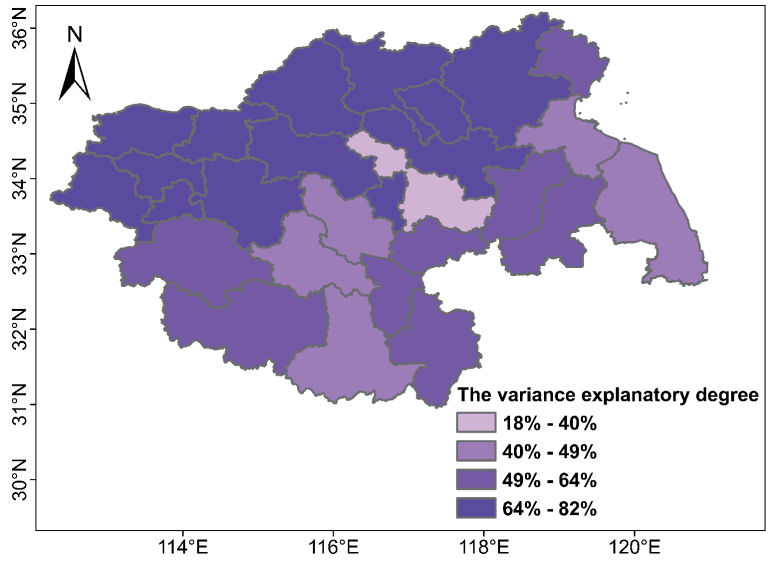

Fig. 7. Influence of meteorological factors on O_3 concentrations in the HREB.

low precipitation, mainly concentrated in the summer, which caused a non-significant relationship between O_3 concentration and Pre. The correlation of O_3 vs. WS and O_3 vs. WD was insignificant in all cities.

The MLR was used to determine the influence of meteorological conditions on O_3 concentration in each city in the HREB from 2015 to 2020. The variance explanation rate reflects the influence of meteorological factors on O_3 concentrations, with a value greater than 50.0% indicating a significant impact. Overall, meteorological factors can explain 82.2%~18.2% (60.5% on average) of the variation in O_3 concentrations in the HREB. There were 21 cities with a variance explanation rate greater than 50%, accounting for 77.8% of all cities in the HREB. Cities with an explanation rate greater than 65.0% were concentrated in the northern part of the HREB. Specifically, Heze had the highest value (0.82). In Bozhou, Luan, Suizhou, Yancheng, Lianyungang, and Fuyang, meteorological factors have a relatively weak impact on O_3 changes. In the northern part of the HREB, many industries are discharging massive anthropogenic pollutants [42]. Further, the northern part of the HREB is relatively flat and susceptible to monsoon winds [43]. These reasons all contributed to the high O_3 concentration in the northern HREB. It is necessary to consider the specific influence of meteorological factors in different seasons in developing O_3 pollution control measures.

Conclusion

In this study, the spatiotemporal distributions of O_3 and the meteorological driving forces on O_3 in the HREB were investigated using various interdisciplinary methods such as geographic analysis and spatial statistics. The results revealed that the annual average by 8.9% in 2020 (163.0 μg/m^3) compared to 2018. O pollution remained an urgent issue in the HREB. The O_3 concentration showed a bimodal variation with month, with the highest level in June (155.3 μg/m^3). In season, O_3 concentrations in the HREB displayed a characteristic of being high in spring and summer and low in autumn and winter. The daily variation of O_3 increased during the day and decreased at night. The maximum daily O_3 concentration occurred at 15:00 (LT) and the minimum at 7:00. In terms of spatial distribution, O_3 concentrations in the HREB were mainly distributed in the southwest-northeast direction. SDE detected that the center of O_3 concentration was in southeastern Shangqiu (33.80°N-33.89°N, 116.33°E-116.40°E). From 2015 to 2020, the center first moved southeast and then northwest. O_3 concentration in the HREB showed positive spatial autocorrelation. The strongest spatial autocorrelation was found in the autumn. The most polluted cities were distributed in the northern HREB, including Heze, Jining, and Zaozhuang, forming a high-high (HH) aggregation. The cities in the southern HREB, including Huainan, Luan, and Hefei, have low O_3 concentrations and have formed low-low (LL) clustering. O_3 was positively correlated with *T* and SSD and negatively correlated with *P*, RH, and Pre in most cities. Meteorological factors can explain 82.2%~18.2% (60.5% on average) of the variation in O_3 concentrations in the HREB. The O_3 in the northern HREB was more affected by meteorological conditions than in the southern HREB.

Acknowledgments

This work was Supported by National Natural Science Foundation of China (Grant No. 41771438), the Program for Innovative Research Team (in Science

and Technology) in University of Henan Province (Grant No. 22IRTSTHN010), the Key Scientific and Technological Research Project of Henan Province (Grant No. 232102320130), and the Nanhu Scholars Program for Young Scholars of Xinyang Normal University.

Conflict of Interest

The authors declare no conflict of interest.

References

1. MUNIR R., KHAYYAM U. China-Pakistan Economic Corridor and the Impact of Coal-Based Energy Projects on Tropospheric Ozone in Pakistan. Polish Journal of Environmental Studies. **29** (5), 3729, **2020**.
2. LIU X., ZHU Y.J., XUE L., DESAI A.R., WANG H.K. Cluster-Enhanced Ensemble Learning for Mapping Global Monthly Surface Ozone From 2003 to 2019. Geophysical Research Letters. **49** (11), e2022GL097947, **2022**.
3. HOU Y.J., SHEN Z. Research Trends, Hotspots and Frontiers of Ozone Pollution from 1996 to 2021: A Review Based on a Bibliometric Visualization Analysis. Sustainability. **14** (17), 10898, **2022**.
4. LI A., ZHOU Q., XU Q. Prospects for ozone pollution control in China: An epidemiological perspective. Environmental Pollution. **285**, 117670, **2021**.
5. WANG Z.S. Satellite-Observed Effects from Ozone Pollution and Climate Change on Growing-Season Vegetation Activity over China during 1982-2020. Atmosphere. **12** (11), 1390, **2021**.
6. JIANG Y.P., ZHU A.D., JIANG S.W., LI Z.G., YANG C.Z. Evaluation of O_3 and NO_x Pollution Based on People's Perception. Polish Journal of Environmental Studies. **31** (1), 979, **2022**.
7. ZHENG D.Y., HUANG X.J., GUO Y.H. Spatiotemporal variation of ozone pollution and health effects in China. Environmental Science and Pollution Research. **29** (38), 57808, **2022**.
8. YU R.L., LIN Y.L., ZOU J.H., DAN Y.B., CHENG C. Review on Atmospheric Ozone Pollution in China: Formation, Spatiotemporal Distribution, Precursors and Affecting Factors. Atmosphere. **12** (12), 1675, **2021**.
9. JIN X.M., HOLLOWAY T. Spatial and temporal variability of ozone sensitivity over China observed from the Ozone Monitoring Instrument. Journal of Geophysical Research-Atmospheres. **120** (14), 7229, **2015**.
10. WANG X., GU W.H., WANG F., LIU L., WANG Y., HAN X.M., XIE Z.Q. A potential controlling approach on surface ozone pollution based upon power big data. SN Applied Sciences. **4** (6), 164, **2022**.
11. YANG X., CHENG X., YAN H. Z., SUN Y.M., ZHANG G.Q. Ground-Level Ozone Production over an Industrial Cluster of China: a Box Model Analysis of a Severe Photochemical Pollution Episode. Polish Journal of Environmental Studies. **31** (2), 1885, **2022**.
12. KONG D.M., LIANG J.W., LIU C.H. Invisible enemy: The health impact of ozone. China Economic Review. **72**, 101760, **2022**.
13. WANG Y.P., WANG H.Y., WANG W.K. A Stratospheric Intrusion-Influenced Ozone Pollution Episode Associated with an Intense Horizontal-Trough Event. Atmosphere. **11** (2), 164, **2020**.
14. WU G.L., SAHABUDDIN M., BHATTI U.A., NAWAZ S.A., HASNAIN A., BHATTI M.A., FAHIM A., KALERI A.A., KALERI A.H. COVID-19 and Air Pollution: Air Quality Impact in 13 Cities of the Jiangsu Province of China. Polish Journal of Environmental Studies. **31** (5), 4907, **2022**.
15. LU Y., SHAO M., ZHENG C.H., JI H.B., GAO X., WANG Q.G. Air pollutant emissions from fossil fuel consumption in China: Current status and future predictions. Atmospheric Environment. **231**, 117536, **2020**.
16. KIM C.S., ALEXIS N.E., RAPPOLD A.G., KEHRL H., HAZUCHA M.J., LAY J.C., SCHMITT M.T., CASE M., DEVLIN R.B., PEDEN D.B., DIAZ-SANCHEZ D. Lung Function and Inflammatory Responses in Healthy Young Adults Exposed to 0.06 ppm Ozone for 6.6 Hours. American Journal of Respiratory and Critical Care Medicine. **183** (9), 1215, **2011**.
17. WANG C.C., LIN Q.Q., QIU Y. Productivity loss amid invisible pollution. Journal of Environmental Economics and Management. **112**, 102638, **2022**.
18. ZHANG X.X., ZHANG X.F., ZHANG L., ZHANG Y.C., ZHANG D., GU X., ZHENG Y.H., WANG T.Z., LI C.H. Metabolite profiling for model cultivars of wheat and rice under ozone pollution - ScienceDirect. Environmental and Experimental Botany. **179**, 104214, **2020**.
19. WANG Y.L., WILD O., ASHWORTH K., CHEN X.S., WU Q.Z., QI Y., WANG Z.F. Reductions in crop yields across China from elevated ozone. Environmental Pollution. **292**, 118218, **2022**.
20. SARKAR M., PANDEY D., RAKWAL R., AGRAWAL G.K., SARKAR A. Impact of tropospheric ozone pollution on wheat production in Southeast Asia: An update. Global Climate Change. Elsevier, 235, **2021**.
21. XU X.B. Recent advances in studies of ozone pollution and impacts in China: A short review. Current Opinion in Environmental Science & Health. **19**, 100225, **2021**.
22. LU X., HONG J.Y., ZHANG L., COOPER O.R., SCHULTZ M.G., XU X.B., WANG T., GAO M., ZHAO Y.H., ZHANG Y.H. Severe Surface Ozone Pollution in China: A Global Perspective. Environmental Science & Technology Letters. **5** (8), 487, **2018**.
23. LIU X.Y., ZHANG Y.D., YAN J.H., ZHANG X.M., ZHAO C.M. Assessing the Influence of Anthropogenic Emissionsons on Fine Particulate Matter and Ozone in Xinyang. Journal of Xinyang Normal University (Natural Science Edition). **36** (02), 190, **2023**.
24. LATIF M.T., HUEY L.S., JUNENG L. Variations of surface ozone concentration across the Klang Valley, Malaysia. Atmospheric Environment. **61**, 434, **2012**.
25. TANG G.Q., LIU Y.T., HUANG X., WANG Y.H., HU B., ZHANG Y.C., SONG T., LI X.L., WU S., LI Q.H., KANG Y.Y., ZHU Z.Y., WANG M., WANG Y.M., LI T.T., LI X., WANG Y.S. Aggravated ozone pollution in the strong free convection boundary layer. Science of the Total Environment. **788**, 147740, **2021**.
26. HU Z.Z., TANG X.G., ZHENG C., GUAN M.L., SHEN J.W. Spatial and temporal analyses of air pollutants and meteorological driving forces in Beijing-Tianjin-Hebei region, China. Environmental Earth Sciences. **77** (14), 1, **2018**.
27. WANG T., XUE L.K., FENG Z.Z., DAI J.N., ZHANG Y.N., TAN Y. Ground-level ozone pollution in China: a synthesis of recent findings on influencing factors and

impacts. Environmental Research Letters. **17** (6), 063003, **2022**.
28. WANG H.W., GAO Y., SHENG L.F., WANG Y.H., ZENG X.R., KOU W.B., MA M.C., CHENG W.X. The Impact of Meteorology and Emissions on Surface Ozone in Shandong Province, China, during Summer 2014-2019. International Journal of Environmental Research and Public Health. **19** (11), 6758, **2022**.
29. YAO S.Y., WEI W., SHEN Z.Y., WANG C.D., NIU Y. Source apportionment of ozone pollution in the typical steel industry city of China in summer. China Environmental Science. **41** (1), 37, **2021**.
30. LIU X.Y., ZHAO C.M., NIU J.Q., SU F.C., YAO D., XU F., YAN J.H., SHEN X.Z., JIN T. Spatiotemporal Patterns and Regional Transport of Ground-Level Ozone in Major Urban Agglomerations in China. Atmosphere. **13** (2), 301, **2022**.
31. SONG M.L., XIE Q.J. Evaluation of Urban Competitiveness of the Huaihe River Eco-Economic Belt Based on Dynamic Factor Analysis. Computational Economics. **58** (3), 615, **2021**.
32. CAO Y.H., XIA Y.X., MAO G.X., CAI A.N., LIU C.M. Research on Regional Development Difference and Collaborative Development Strategy of the Huaihe River Eco-economic Belt. Economic Geography. **39** (9), 213, **2019**.
33. LIU X.Y., GAO H., ZHANG X.M., ZHANG Y.D., YAN J.H., NIU J.Q., CHEN F.Y. Driving Forces of Meteorology and Emission Changes on Surface Ozone in the Huaihe River Basin, China. Water Air and Soil Pollution. **234 (**6), 355, **2023**.
34. LIU X.Y., NIU J.Q., YAN J., YAN J.H., ZHAO C M., XU F., ZHANG Y.D., ZHANG B.B. Surface Ozone in the Central Plains Urban Agglomeration, China: Spatial-Temporal Variations and Health Impacts. Polish Journal of Environmental Studies. **31** (5), 4767, **2022**.
35. YAN J., CUI R.P. Study on Spatial-temporal Differentiation and Convergence of Tourism Economy in the Huaihe River Eco-economic Belt. Areal Research and Development. **39** (4), 91, **2020**.
36. JIANG L., HE S.X., ZHOU H.F. Spatio-temporal characteristics and convergence trends of PM2.5 pollution: A case study of cities of air pollution transmission channel in Beijing-Tianjin-Hebei region, China. Journal of Cleaner Production. **256**, 120631, **2020**.
37. HUANG J.W., SONG L., YU M., ZHANG C.J., LI S.P., LI Z.X., GENG J., ZHANG C. Quantitative spatial analysis of thermal infrared radiation temperature fields by the standard deviational ellipse method for the uniaxial loading of sandstone. Infrared Physics & Technology. **123**, 104150, **2022**.
38. ANSELIN L. Local Indicators of Spatial Association – LISA. Geographical Analysis. **27** (2), 93, **1995**.
39. BOOTS B., TIEFELSDORF M. Global and local spatial autocorrelation in bounded regular tessellations. Geographical Systems. **2**, 319, **2000**.
40. YIN C.Q., SOLMON F., DENG X.J., ZOU Y., DENG T., WANG N., LI F., MAI B.R., LIU L. Geographical distribution of ozone seasonality over China. Science of The Total Environment. **689**, 625, **2019**.
41. TOUATI H., GUERIN A., SWESI Y., DUPEYRAT C.B., PHILIPPE R., MEILLE V., CLACENS J.M. Unexpected role of NO_x during catalytic ozone abatement at low temperature. Catalysis Communications. **148**, 106163, **2021**.
42. WIE J., PARK H.J., LEE H., MOON B.K. Near-Surface Ozone Variations in East Asia during Boreal Summer. Atmosphere. **11** (2), 206, **2020**.
43. LIU P.F., SONG H.Q., WANG T.H., WANG F., LI X.Y., MIAO C.H., ZHAO H.P. Effects of meteorological conditions and anthropogenic precursors on ground-level ozone concentrations in Chinese cities. Environmental Pollution. **262**, 114366, **2020**.